

# Topological Analysis of the Electron Density in the Carbonyl Complexes $M(\text{CO})_8$ ( $M = \text{Ca}, \text{Sr}, \text{Ba}$ )

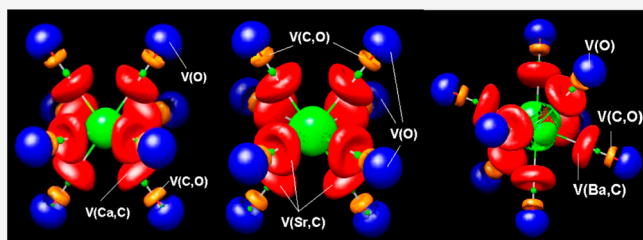
Juan F. Van der Maelen\*<sup>1</sup>

Departamento de Química Física y Analítica, Universidad de Oviedo, E-33006 Oviedo, Spain

Centro de Investigación en Nanomateriales y Nanotecnología (CINN-CSIC), E-33940 El Entrego, Spain

## Supporting Information

**ABSTRACT:** The quantum theory of atoms in molecules (QTAIM) has been applied to the recently synthesized alkaline-earth cubic  $O_h$ -symmetric complexes  $\text{Ca}(\text{CO})_8$  (1),  $\text{Sr}(\text{CO})_8$  (2), and  $\text{Ba}(\text{CO})_8$  (3). Theoretical calculations reveal that  $M\text{--CO}$  interactions in these complexes can be properly described as highly polar bonds, showing some features traditionally associated with transition-metal bonding, although with noticeable differences, as well. In this sense,  $\delta(M\text{--C})$  and  $\delta(M\cdots\text{O})$  delocalization indexes for bonding and nonbonding interactions, electron localization function (ELF) analyses, source function (SF) calculations, and the interacting quantum atoms (IQA) approach, among other methodologies, produce results consistent with interactions dominated by electrostatics between the CO ligands and alkaline-earth metals, with an increasing degree of covalency on going from 1 to 3 and without any significant  $\pi$ -back-donation.



## INTRODUCTION

The study of the bonding between metal atoms and CO ligands has a long tradition in chemistry, and it is essential to understand reactivity, surface chemistry, and catalysis.<sup>1</sup> The most commonly used description of  $M\text{--CO}$  bonding when  $M$  = transition metal (TM) uses the Dewar–Chatt–Duncanson model (DCD), namely,  $\sigma$ -donation from the CO group to an empty orbital of the TM and  $\pi$ -back-donation from the TM to a  $\pi^*$  orbital of the CO group.<sup>2</sup> The back-bonding into the unoccupied  $\pi^*$  orbital of the CO group is used as well to explain the CO stretch frequency red shift of the so-called “classical” carbonyl complexes,<sup>3</sup> which represent the great majority of TM carbonyl complexes. In nonclassical carbonyl complexes, the  $\pi$ -back-bonding is of less importance, resulting in no red shift or even leading to a blue shift.<sup>4</sup> Recently, the synthesis and spectroscopic characterization of the complexes  $\text{Ca}(\text{CO})_8$ ,  $\text{Sr}(\text{CO})_8$ , and  $\text{Ba}(\text{CO})_8$ , followed by a theoretical electron density analysis (EDA-NOCV),<sup>5</sup> led the authors to conclude that the DCD model is also valid to explain the  $M\text{--CO}$  bonding in these alkaline-earth compounds, as well as the strong observed red shift of their  $\text{C}\text{--O}$  stretching frequencies.<sup>6</sup> However, this conclusion is far from being clear as other authors have claimed that the flexibility in the chosen starting reference state needed for EDA calculations may well be misleading, as an alternative EDA analysis using a different reference state leads exactly to the opposite conclusion; that is, the simple DCD model is not valid to explain the bonding in these alkaline-earth carbonyls.<sup>7</sup> In addition, a recent density functional theory (DFT) study on  $\text{Mg}(\text{CO})_8$ ,  $\text{Ca}(\text{CO})_8$ , and  $\text{Ti}(\text{CO})_8^{2+}$  has found a considerable CO red shift without the presence of metal–carbon  $\pi$ -bonds in the  $\text{Mg}(\text{CO})_8$  cluster,

leading to the general conclusion that the CO red shift in metal–carbonyl bonds is not always dependent on d functions alone, although the presence of d functions and the formation of  $M\text{--C}$   $\pi$ -bonds does always increase the covalency of the metal–CO interaction.<sup>8</sup>

In order to shed some additional light on the nature of the bonding on this important class of compounds, we have used the quantum theory of atoms in molecules (QTAIM),<sup>9</sup> as well as the electron localization function approach (ELF),<sup>10</sup> which are two different and complementary ways of partitioning the molecular electron density. As opposed to the molecular orbital (MO) theory, these approaches are based on the electron density (a real space function), which is an observable that may be obtained either from X-ray data or theoretical calculations. Both QTAIM and ELF methodologies, combined with other related to them, like the source function (SF)<sup>11</sup> and the interacting quantum atoms approach (IQA),<sup>12</sup> have been applied so far to a plethora of organometallic compounds, with and without transition metals, giving unambiguous, stable, and robust results, which are almost independent of the model chemistry used (i.e., method of calculation, density functional, and basis set).<sup>13</sup> Previously published theoretically optimized structures of 1, 2, and 3 in their ground states (triplet states,  $O_h$  symmetry) were used in the present study in order to obtain results more directly comparable to the ones of Wu et al. (see Table S1 in the Supporting Information for tables of coordinates).<sup>5</sup> Four theoretical models have been utilized (see the Experimental Section for details), which in the

Received: October 18, 2019

Published: December 24, 2019

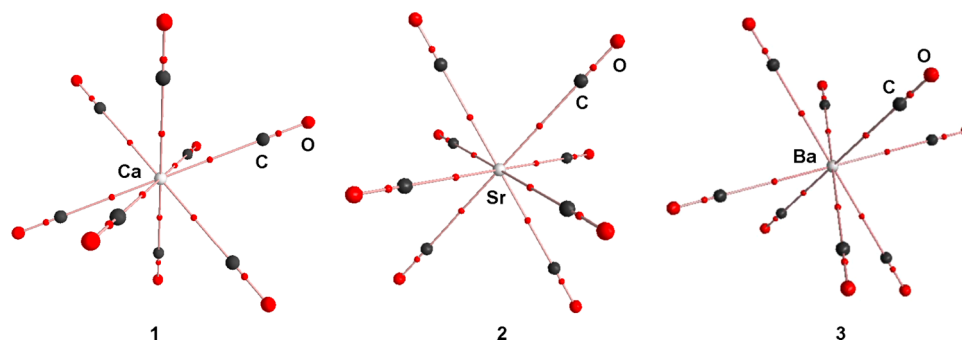


**Figure 1.** Molecular graph of **1**, **2**, and **3**, showing bond critical points (small red spheres) and bond paths (thin lines).

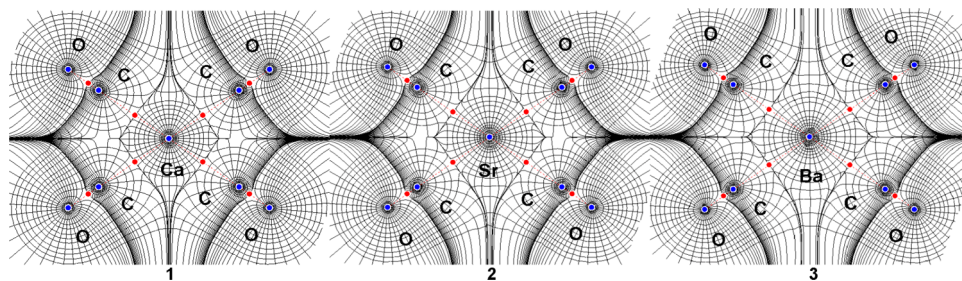


**Figure 2.** Gradient trajectories mapped on total electron density plots (contour levels at  $0.1 e \text{ \AA}^{-3}$ ) in C–M–C planes of compounds **1**, **2**, and **3**, showing atomic basins, stationary points (blue circles), bps (red lines), and bcps (red circles).

following will be denoted as follows: SO-M06-2X/QZ4P (model 1), SO-B3LYP-D3/QZ4P (model 2), M06-D3/6-311++G(3df,3pd),DKH3-QZP (model 3), and B3P86-D3/6-311++G(3df,3pd),DKH3-QZP (model 4). The four models use all-electron basis sets for all atoms (including metal atoms), but whereas the first two models utilize a fully relativistic Hamiltonian with spin–orbit (SO) terms,<sup>14</sup> the last two models use a nonrelativistic Hamiltonian.

## RESULTS AND DISCUSSION

The images in **Figure 1** show all atoms corresponding to each complex and the complete set of bond critical points (bcps), as well as bond paths (bps) connecting bonded atoms through their corresponding bcps. From the orthodox QTAIM point of view, the presence of a bp and a bcp between two atoms is a necessary and sufficient condition for the existence of a bonding interaction between both atoms,<sup>9a</sup> although it is well-known that alternative interpretations are also possible, particularly when weak and very weak interactions are involved.<sup>13e</sup> Two main features, which these complexes have in common with TM–CO compounds,<sup>15</sup> may be appreciated from **Figure 1**. First, bps in the three complexes are perfectly straight lines, meaning that no significant differences between bond path lengths and interatomic distances are found (see below for a more quantitative discussion of this point). Second, whereas M–C bcps are located approximately at the midpoints of their corresponding bps, C–O bcps are clearly closer to C atoms than to O atoms (the Supporting Information gives the exact M–bcp, bcp–C, C–bcp, and bcp–O distances in **Table S2**).

In **Figure 2**, gradient trajectory maps of the total electron density in a C–M–C plane of complexes **1**, **2**, and **3** are shown, where the atomic basins of Ca, Sr, and Ba, respectively, are displayed (CO ligands are also shown). Differences in the size of metal-atom basins may be clearly appreciated from

**Figure 2**, whereas basins for C and O atoms are basically identical in the three complexes, as expected.

Atomic electric charges are obtained by integration of the electron density inside each atomic basin. In **Table 1** a

**Table 1.** Atomic Charges,  $Q(A)$  ( $e$ ), for All Atoms in Compounds **1**, **2**, and **3**<sup>a</sup>

complex	M <sup>b</sup>	C	O
<b>1</b>	1.415	1.013	−1.190
	1.523	0.934	−1.125
	1.437	0.994	−1.173
	1.463	0.988	−1.171
<b>2</b>	1.422	1.010	−1.188
	1.496	0.973	−1.170
	1.401	0.998	−1.173
	1.433	0.992	−1.171
<b>3</b>	1.354	1.025	−1.194
	1.430	0.994	−1.172
	1.231	1.023	−1.176
	1.293	1.015	−1.175

<sup>a</sup>Models: SO-M06-2X/QZ4P (first row), SO-B3LYP-D3/QZ4P (second row), M06-D3/6-311++G(3df,3pd),DKH3-QZP (third row), and B3P86-D3/6-311++G(3df,3pd),DKH3-QZP (fourth row). <sup>b</sup>M = Ca (**1**), Sr (**2**), Ba (**3**).

comparison between QTAIM charges of all atoms in **1**, **2**, and **3** using the four theoretical models is made, showing small differences between nonrelativistic and relativistic models in the case of complexes **1** and **2** but significant differences for the Ba atom in complex **3**, as expected. In the three complexes, the metal center has a zero formal oxidation state and the atomic charge for the metal atom is approximately +1.4  $e$ , which is about 50% higher than typical values found for transition metals in carbonyl compounds. For instance, using similar calculation methods, Mn, Tc, and Re atomic charges in

$M_2(CO)_{12}$  complexes are between +0.9 and +1.1  $e$ ,<sup>15f</sup> Os charges in  $Os_3(CO)_{12}$ ,  $Os_3(\mu-H)_2(CO)_{10}$ ,  $Os_3(\mu-H)(\mu-OH)(CO)_{10}$ , and  $Os_3(\mu-H)(\mu-Cl)(CO)_{10}$  are between +0.75 and +1.0  $e$ ,<sup>15g</sup> and V, Cr, Mn, and Fe charges in the highly symmetric octahedral complexes  $[V(CO)_6]^-$ ,  $Cr(CO)_6$ ,  $[Mn(CO)_6]^+$ , and  $[Fe(CO)_6]^{2+}$ , respectively, are between +0.9 and +1.2  $e$ ,<sup>15j</sup> among many other instances in the given references. The Coulomb electrostatic potential (ESP), represented in Figure 3, is even more informative than monopolar charges alone as it includes multipolar expansion terms, showing a clear separation between metal and CO charges in the three complexes. These results are consistent with a high electrostatic contribution to the M–CO bonding interaction in 1, 2, and 3.

Local topological properties of the electron density (i.e., those calculated at a bcp) have been frequently used to successfully analyze the bonding in all kinds of compounds, particularly those containing metal atoms. The electron density ( $\rho_b$ ), the ellipticity ( $\epsilon_b$ ), the Laplacian of the electron density ( $\nabla^2\rho_b$ ), the kinetic energy density ratio ( $G_b/\rho_b$ ), and the total energy density ratio ( $H_b/\rho_b$ , with  $H(r) = G(r) + V(r)$  and  $1/4\nabla^2\rho(r) = 2G(r) + V(r)$ , where  $V(r)$  is the potential energy density) are the most common of those properties.<sup>13,15</sup> Generally speaking, local topological properties are related to the strength and nature of the interactions for which a bcp is present and may be used to classify bonds between the traditional chemical categories, that is, closed-shell versus open-shell, as well as to distinguish between pure covalent, polar covalent, dative, and ionic bonds, among others.<sup>15</sup> For metal–ligand bonds, like an M–C interaction, a typical donor–acceptor covalent bond has a relatively small value of  $\rho_b$ , a relatively large and positive value of  $\nabla^2\rho_b$ , a negative value of  $H_b/\rho_b$  (with  $|H_b/\rho_b| < 1$ ), and a value greater than 1 of  $G_b/\rho_b$ . The ellipticity, which measures the deviation from a perfect cylindrical symmetry ( $\epsilon = 0$ ) of the electron density along a bp, can take any value for a general metal–ligand interaction, being usually zero for TM–CO bonds.

In Table 2, values of the above-mentioned local topological properties for all bonds of complexes 1, 2, and 3, and using the four theoretical models, are included. As may be seen in Table 2, the ellipticity is 0 for both M–C and C–O bcps, which is because the eigenvalues of the electron density's Hessian matrix are degenerate due to the symmetry of the three molecules. As mentioned above, it is noteworthy that M–C bond path lengths in 1, 2, and 3 are exactly equal to their interatomic distances (tables of interatomic distances are given in Table S2 of the Supporting Information), which added to the exactly 0 values for  $\epsilon_b$ , confirms that they are cylindrical straight bond paths, with no curvature at all, like the ones found in many typical TM–CO bonds.<sup>15</sup> However, the small ( $<1$ ) values of  $\rho_b$ , added to the small positive values of  $\nabla^2\rho_b$ , the small ( $<1$ ) positive values for  $H_b/\rho_b$ , and the  $<1$  values of  $G_b/\rho_b$ , shown by all M–C bonds in Table 2, are typical of weak donor–acceptor interactions of a high electrostatic nature. As a comparison, a typical TM–CO interaction, like Ru–CO bonds in the triruthenium cluster  $[Ru_3(\mu-H)_2(\mu_3-\kappa^2-MeImCH)(CO)_9]$  ( $Me_2Im = 1,3$ -dimethylimidazol-2-ylidene),<sup>15a</sup> has  $\rho_b = 0.951 e \text{ \AA}^{-3}$  (more than 5 times greater than that in 1–3),  $\nabla^2\rho_b = 13.304 e \text{ \AA}^{-5}$  (again, more than 5 times greater than that in 1–3),  $H_b/\rho_b = -0.393 h e^{-1}$  (a negative value, typical of open-shell interactions), and  $G_b/\rho_b = 1.372 h e^{-1}$  (greater than 1), with results very similar in many other published transition-metal carbonyl compounds.<sup>13,15</sup>

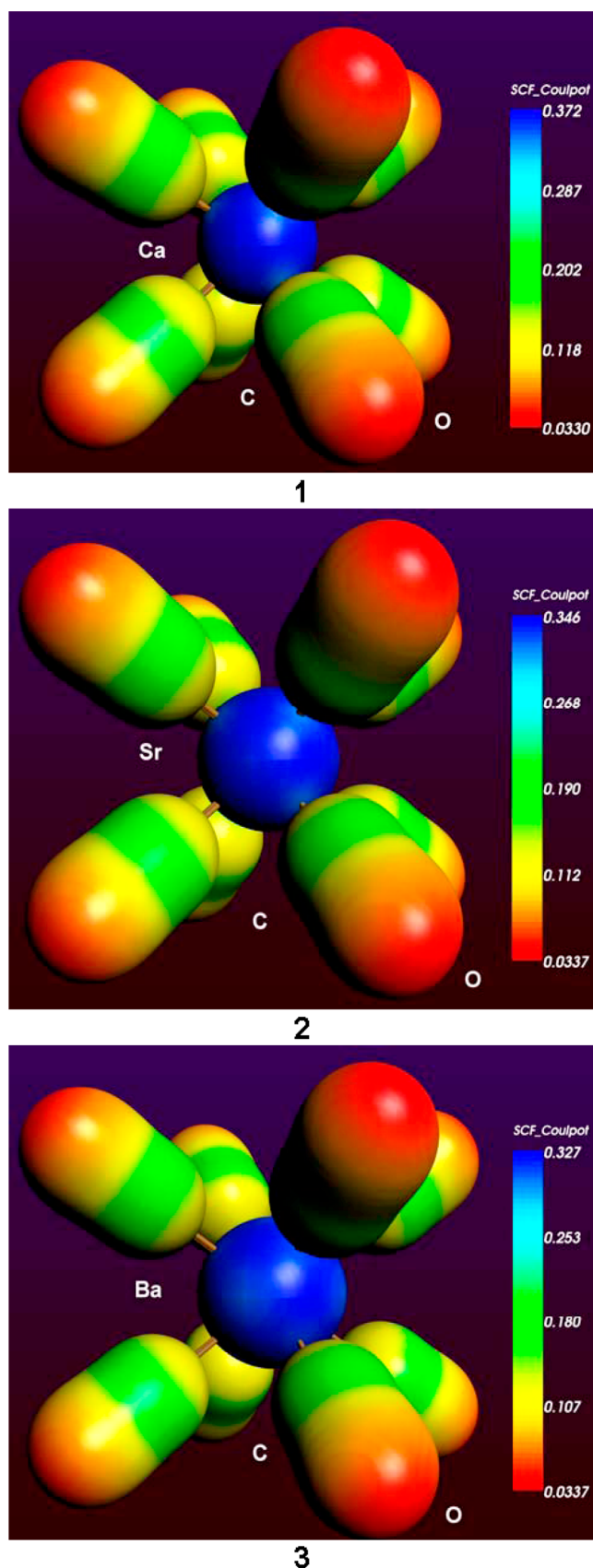


Figure 3. Electrostatic potential (au) mapped on a  $0.03 e \text{ \AA}^{-3}$  electron density isosurface for 1, 2, and 3.

Table 2. QTAIM Local and Integral Properties for Bonding Interactions of Complexes 1, 2, and 3<sup>a</sup>

bond <sup>b</sup>	complex	<i>d</i> (Å) <sup>c</sup>	$\rho_b$ ( <i>e</i> Å <sup>-3</sup> ) <sup>d</sup>	$\nabla^2\rho_b$ ( <i>e</i> Å <sup>-5</sup> ) <sup>e</sup>	$H_b/\rho_b$ (h <i>e</i> <sup>-1</sup> ) <sup>f</sup>	$G_b/\rho_b$ (h <i>e</i> <sup>-1</sup> ) <sup>g</sup>	$\epsilon_b$ <sup>h</sup>	$\delta(A-B)$ <sup>i</sup>
M–C	1	2.602	0.172	2.636	0.101	0.972	0.000	
		2.600	0.174	2.572	0.094	0.941	0.000	
		2.602	0.171	2.714	0.125	0.986	0.000	0.162
		2.600	0.172	2.747	0.130	1.013	0.000	0.159
	2	2.752	0.162	2.256	0.082	0.893	0.000	
		2.751	0.165	2.190	0.075	0.854	0.000	
		2.752	0.163	2.176	0.075	0.860	0.000	0.185
		2.751	0.167	2.186	0.069	0.847	0.000	0.181
	3	2.960	0.141	1.776	0.065	0.817	0.000	
		2.964	0.146	1.706	0.077	0.741	0.000	
		2.960	0.145	1.836	0.084	0.802	0.000	0.230
		2.964	0.148	1.839	0.078	0.792	0.000	0.223
C–O	1	1.127	3.409	12.349	–1.970	2.224	0.000	-----
		1.134	3.464	12.348	–1.955	2.205	0.000	-----
		1.127	3.415	4.196	–1.967	2.053	0.000	1.696
		1.134	3.450	7.208	–2.001	2.147	0.000	1.700
	2	1.126	3.417	11.944	–1.972	2.217	0.000	
		1.134	3.469	11.943	–1.962	2.203	0.000	
		1.126	3.421	4.193	–1.970	2.056	0.000	1.708
		1.134	3.456	7.222	–2.003	2.149	0.000	1.713
	3	1.125	3.419	13.568	–1.965	2.243	0.000	
		1.133	3.465	13.567	–1.951	2.225	0.000	
		1.125	3.432	4.205	–1.973	2.059	0.000	1.719
		1.133	3.466	7.321	–2.006	2.154	0.000	1.725

<sup>a</sup>Models: SO-M06-2X/QZ4P (first row), SO-B3LYP-D3/QZ4P (second row), M06-D3/6-311++G(3df,3pd),DKH3-QZP (third row), and B3P86-D3/6-311++G(3df,3pd),DKH3-QZP (fourth row). <sup>b</sup>M = Ca (1), Sr (2), Ba (3). <sup>c</sup>Bond path length. <sup>d</sup>Electron density at the bcp. <sup>e</sup>Laplacian of the electron density at the bcp. <sup>f</sup>Total energy density ratio at the bcp. <sup>g</sup>Kinetic energy density ratio at the bcp. <sup>h</sup>Ellipticity at the bcp. <sup>i</sup>Delocalization index.

However, it is well-known that integral indexes are even more useful than local indexes for characterizing bonds in compounds containing metal atoms.<sup>9,10</sup> Integral topological properties are calculated along a bond path, over an interatomic surface or over a whole atomic basin. Among them, the delocalization index (DI),  $\delta(A-B)$ , which can be considered a covalent bond order measure as it is directly related to the number of electron pairs shared between atoms A and B, is by far the integral index that has been most frequently used. For metal–ligand bonds, like an M–C interaction, a typical donor–acceptor covalent bond has a value of DI approximately equal to the formal bond order. In Table 2 (last column),  $\delta(A-B)$  values of M–C and C–O bonds for 1, 2, and 3 are included. Although the values obtained for the C–O bonds in these complexes are equivalent to those found in TM–CO compounds, those calculated for M–C bonds are clearly smaller. For instance,  $\delta(M-CO)$  in  $[M_2(CO)_{10}]$  (M = Mn, Tc, Re) lies between 1.12 and 1.19 for axial carbonyls and between 0.94 and 0.99 for equatorial carbonyls, with similar values for trinuclear complexes,<sup>15f</sup>  $\delta(Ru-CO)$  in the above-mentioned  $[Ru_3(\mu-H)_2(\mu_3\kappa^2-MeImCH)(CO)_9]$  complex, as well as in  $[RuH(\kappa^3N,H,H-mapyBH_3)(CO)(P^iPr_3)]$  (Hmapy = 2-(methylamino)-pyridine) are, respectively, 1.089 and 1.413,<sup>15a,e</sup> and  $\delta(Os-CO)$  in several Os carbonyl complexes lies between 1.04 and 1.08,<sup>15g</sup> among many other instances with similar results.<sup>15c,h,i</sup> In all of these instances, the TM–CO bond can be interpreted as a donor–acceptor covalent interaction with a bond order of about unity, which follows the classical DCD model of a key-lock mechanism. On the other hand, for the highly symmetric octahedral TM complexes  $[V(CO)_6]^-$ ,  $Cr(CO)_6$ , and  $[Mn-$

$(CO)_6]^+$ , for which the simple DCD model does not give the complete picture,  $\delta(TM-CO)$  takes the values 0.62, 0.74, and 0.68, respectively, showing nevertheless a high degree of covalency.<sup>15j</sup> Values in Table 2 for  $\delta(M-CO)$  in 1, 2, and 3 clearly show a much lower degree of covalency, which can be estimated to be approximately 16, 18, and 23% for Ca–C, Sr–C, and Ba–C, respectively, from these DIs alone, assuming a DI value of 1 for a formal bond order of 1 in a pure covalent 2c–2e bond without delocalization (see below for a more quantitative discussion on this point).

Detecting  $\pi$ -back-donation from the point of view of QTAIM can be made from the  $\delta(M\cdots O_{CO})$  delocalization index, as  $\pi$ -back-donation involves a significant  $M\cdots O_{CO}$  interaction.<sup>13b</sup> For instance,  $\delta(Cu\cdots O)$  and  $\delta(B\cdots O)$ , respectively, in  $[Cu(CO)_2]^+$  and  $H_3BCO$ , where no  $\pi$ -back-donation exists, are very low, 0.09 and 0.04, respectively. On the other hand,  $\delta(M\cdots O_{CO})$  values for Mn, Fe, Co, Ni, Tc, Ru, Re, and Os carbonyl complexes are much higher, ranging from 0.15 to 0.25.<sup>13,15</sup> Values of the  $\delta(M\cdots O_{CO})$  index calculated for complexes 1, 2, and 3, which are shown in Table 3, are even lower than those of  $\delta(B\cdots O)$  in  $H_3BCO$ , displaying a negligible  $\pi$ -back-donation effect in these compounds. Interestingly enough, for the octahedral complexes  $[V(CO)_6]^-$ ,  $Cr(CO)_6$ , and  $[Mn(CO)_6]^+$ ,  $\delta(M\cdots O_{CO})$  takes the values 0.11, 0.10, and

Table 3. Delocalization Indexes,  $\delta(A\cdots B)$ , for  $M\cdots O$  Nonbonding Interactions in Complexes 1, 2, and 3

model	Ca $\cdots$ O	Sr $\cdots$ O	Ba $\cdots$ O
M06-D3/6-311++G(3df,3pd),DKH3-QZP	0.021	0.023	0.032
B3P86-D3/6-311++G(3df,3pd),DKH3-QZP	0.021	0.024	0.033

0.05, respectively, with similar values for the index  $\delta(C_{CO}\cdots C_{CO})$  between neighboring carbonyl groups, leading the authors to propose a multicenter interaction in these complexes to describe the bonding better than the simple DCD model.<sup>15j</sup> Values of  $\delta(C_{CO}\cdots C_{CO})$  for 1–3 are, respectively, 0.10, 0.08, and 0.07, which are not negligible at all as each CO ligand has three adjacent CO groups at the same distance, showing that CO $\cdots$ CO interactions also play an important role in the bonding of these compounds. On the other hand, for the recently synthesized cation BaCO<sup>+</sup>,<sup>15k</sup>  $\delta(Ba\cdots O)$  gives results between 0.137 and 0.139, calculated in this work using the same calculation methods as used for 1–3, which are certainly close to the typical values exhibited by this index in most transition-metal carbonyl complexes, showing that in this particular case there is indeed a significant  $\pi$ -back-donation, consistent with the DCD model for the Ba–CO bond.

An alternative but related way to study the nature of M–CO interactions is the calculation of bond orders. For nonpolar bonds, the delocalization index is usually very close to Mayer's fuzzy bond order (FBO), but they quantitatively differ for polar bonds. FBO is essentially the DI calculated in fuzzy atomic space.<sup>16</sup> Commonly, the magnitude of FBO is close to the usual Mayer bond order,<sup>17</sup> especially for low polar bonds, but much more stable with respect to the change in basis set. It is also worth noting that Lu's Laplacian bond order (LBO) reflects only the covalent component of a bond, whereas FBO may be regarded as total bond order.<sup>18</sup> Therefore, the difference between LBO and FBO may be used to reveal bond polarity. Analogously, the widely used Wiberg bond order (WBO) tends to overestimate bond order for polar bonds with reference to conventional Mayer's bond order.<sup>19</sup> In Table 4, three types of bond order are shown for M–C and

**Table 4. Bond Orders of Bonding Interactions in 1, 2, and 3**

bond <sup>a</sup>	FBO <sup>b</sup>	LBO <sup>c</sup>	WBO <sup>d</sup>
M–C	0.542	0.103	0.490
	0.639	0.164	0.609
	0.607	0.120	0.626
C–O	2.551	1.762	3.506
	2.555	1.768	3.485
	2.579	1.783	3.535

<sup>a</sup>M = Ca (1) (first row), Sr (2) (second row), and Ba (3) (third row).

<sup>b</sup>Mayer's fuzzy bond order. <sup>c</sup>Lu's Laplacian bond order. <sup>d</sup>Wiberg's bond order. Model: M06-D3/6-311++G(3df,3pd),DKH3-QZP. More values are given in the Supporting Information (Table S3).

C–O bonds in complexes 1–3. As may be seen in Table 4, FBO and WBO values are very similar to each other for M–C bonds and much higher than LBO values, which are even smaller than DI values (see Table 2). Differences between LBO values and both FBO and WBO values can be associated with the high polarity of M–C bonds in the three complexes.

An additional tool for characterizing bonding interactions is the integrated electron density over the whole interatomic surface,  $\int_{A\cap B}\rho$ , which is an integral topological property related to the bond strength.<sup>9–11</sup> Table 5 collects values of this property for M–C and C–O bonds in 1, 2, and 3, showing that the former are between 4 and 5 times weaker than usual TM–CO bonds, whose typical values of this index are between 2.2 and 2.7  $e \text{ \AA}^{-1}$ .<sup>13,15</sup>

**Table 5. Electron Density Integrated over the Interatomic Surface,  $\int_{A\cap B}\rho$  ( $e \text{ \AA}^{-1}$ ), for M–C and C–O Interactions of 1, 2, and 3<sup>a</sup>**

complex	M–C <sup>b</sup>	C–O
1	0.366	3.263
	0.351	3.283
2	0.434	3.257
	0.413	3.280
3	0.699	3.251
	0.679	3.275

<sup>a</sup>Models: M06-D3/6-311++G(3df,3pd),DKH3-QZP (first row) and B3P86-D3/6-311++G(3df,3pd),DKH3-QZP (second row). <sup>b</sup>M = Ca (1), Sr (2), Ba (3).

Another integral property that can be calculated from QTAIM atomic basins is the source function, which represents the contribution, in percentage, of each atomic basin to the electron density at a particular point of the molecule (for instance, at a bcp).<sup>10</sup> In Table 6, the SF% at M–C and C–O

**Table 6. SF Contributions (%) of Each Atom to the Electron Density at the bcp of Bonding Interactions in 1, 2, and 3**

bond	M <sup>a</sup>	C	O
M–C	23.402	−3.383	47.079
	26.736	−3.736	48.535
	29.561	−7.151	51.962
C–O	0.016	40.508	58.936
	0.023	40.558	58.978
	0.036	40.536	59.072

<sup>a</sup>M = Ca (1) (first row), Sr (2) (second row), and Ba (3) (third row). Model: M06-D3/6-311++G(3df,3pd),DKH3-QZP. More values are given in the Supporting Information (Table S4).

bcps of each atom is included for complexes 1, 2, and 3. Not surprisingly, almost a 100% of the contribution at each C–O bcp in 1–3 comes from the two bonded atoms (C and O), with only a very small contribution from the metal and from the other CO groups (less than 0.5% in total). Rather interestingly, in M–C bonds of 1–3, the bonded C atom acts as a sink (negative contribution) instead of as a source, where the additional positive contributions (apart from the C-bonded M and O atoms) come from the other CO ligands, not bonded to the C atom. In typical TM–CO interactions, the contribution from the bonded C atom to the M–C bcp is usually high and positive. For instance, in Mn<sub>2</sub>(CO)<sub>10</sub> the SF contributions from Mn, C, and O atoms to each Mn–C bcp are, respectively, 32.65, 34.78, and 12.51%; in Tc<sub>2</sub>(CO)<sub>10</sub>, the equivalent contributions from Tc, C, and O atoms are, respectively, 36.18, 33.83, and 13.18%, and in Re<sub>2</sub>(CO)<sub>10</sub>, they are 36.91, 34.45, and 12.22%, respectively, for Re, C, and O atoms.<sup>15f</sup> For the BaCO<sup>+</sup> cation, the contributions calculated in this work are, respectively, 50.73, 15.19, and 34.08%, which are consistent with a typical Ba–CO covalent bond. On the contrary, the negative SF contribution of C atoms to the electron density at M–C bcps in 1–3 is a clear sign of an interaction dominated by electrostatics.<sup>11,13d</sup>

The interacting quantum atoms approach adopts the real space partition of QTAIM to obtain intra- and interatomic energy contributions from the atomic basins.<sup>12</sup> As opposed to traditional energy decomposition analyses, like EDA-NOCV, it is not necessary to define ambiguous fragments or reference

states to perform the calculations as the atomic basins are already given by the underlying QTAIM approach. In this way, it is possible to partition the interaction energy between two atomic basins, A and B (which can represent either bonded or nonbonded atoms),  $E_{\text{int}}^{\text{AB}}$ , into a classical term,  $V_{\text{cl}}^{\text{AB}}$ , and an exchange-correlation term,  $V_{\text{xc}}^{\text{AB}}$ :  $E_{\text{int}}^{\text{AB}} = V_{\text{cl}}^{\text{AB}} + V_{\text{xc}}^{\text{AB}}$ .  $V_{\text{cl}}^{\text{AB}}$  and  $V_{\text{xc}}^{\text{AB}}$  can be associated with the electrostatic and covalent contributions to the interaction energy, respectively, which can be either negative (stabilizing interaction) or positive (destabilizing interaction).<sup>15j,20</sup> Table 7 collects both con-

**Table 7. IQA Contributions (kcal mol<sup>-1</sup>) to the Bonding Interaction Energy ( $E_{\text{int}}^{\text{AB}}$ ) in 1, 2, and 3**

interaction <sup>a</sup>	$V_{\text{cl}}^{\text{AB}}$	$V_{\text{xc}}^{\text{AB}}$
M–C	122.611	–18.733
	117.024	–20.521
	102.304	–23.172
C–O	–699.709	–299.452
	–703.590	–300.431
	–715.873	–301.222
M···O	–164.842	–1.060
	–154.204	–1.149
	–129.028	–1.450

<sup>a</sup>M = Ca (1) (first row), Sr (2) (second row), and Ba (3) (third row). Model: M06-D3/6-311++G(3df,3pd),DKH3-QZP. More values are given in the Supporting Information (Table S5).

tributions to the interaction energy for M–C, C–O, and M···O interactions in complexes 1–3. Notwithstanding, each destabilizing M–C interaction is quite large, due to the substantial positive charges on both M and C atoms (Table 1); the three molecules are stable thanks to the stabilizing C–O and M···O interactions, the former a typical polar bond (70% electrostatics and 30% covalent) and the latter almost pure electrostatics (more than 99%). By adding the values in Table 7 for M–C and M···O interactions, the covalent contribution to each M–CO bond can be estimated to be 32% for Ca–CO, 37% for Sr–CO, and 48% for Ba–CO, which are lower than those found in typical transition-metal carbonyl complexes. For instance, TM–CO interactions in complexes [Fe(CO)<sub>4</sub>]<sup>2-</sup>, [Co(CO)<sub>4</sub>]<sup>-</sup>, Ni(CO)<sub>4</sub>, and [Co<sub>6</sub>X(CO)<sub>16</sub>]<sup>-</sup> (X = As, P) are clearly dominated by the covalent contribution, whereas for the octahedral complexes [Ti(CO)<sub>6</sub>]<sup>2-</sup>, [V(CO)<sub>6</sub>]<sup>-</sup>, Cr(CO)<sub>6</sub>, [Mn(CO)<sub>6</sub>]<sup>+</sup>, and [Fe(CO)<sub>6</sub>]<sup>2+</sup>, both contributions (covalent and electrostatic) play a similar role.<sup>20,21</sup>

A complementary way to the QTAIM partitioning of the molecular electron density is given by the ELF approach, which is a measure of the likelihood of finding an electron in the neighborhood of a reference electron.<sup>22</sup> ELF provides a useful method for mapping the electron pair probability, and it is usually considered a kind of visualization of VSEPR theory as it shows a clear separation in shells between core and valence electrons, as well as clearly visualizes covalent bonds and lone pairs, among other features. Dimensionless ELF ( $0 \leq \eta \leq 1$ ) of the Ba complex is depicted in Figure 4, where disynaptic valence basins,  $V(\text{Ba,C})$  and  $V(\text{C,O})$ , corresponding to Ba–C and C–O interactions, are shown, as well as monosynaptic basins located at carbonyl O atoms,  $V(\text{O})$ , corresponding to lone pairs (similar figures for Ca and Sr complexes are included in Figure S1 of the Supporting Information). Despite the fact that bonding basins  $V(\text{Ba,C})$  have a disynaptic character, this is mainly a closed-shell interaction, according to the distances

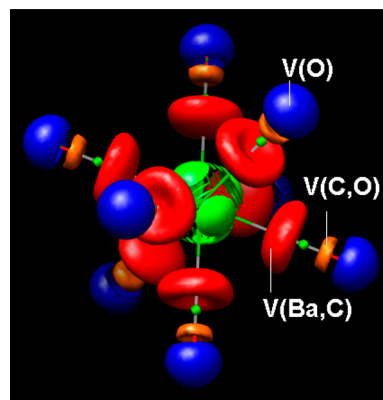


**Figure 4.** Electron localization function isosurface at  $\eta = 0.8$  for the Ba(CO)<sub>8</sub> complex. Color codes: green for C(Ba), C(C), and C(O); red for  $V(\text{Ba,C})$ ; orange for  $V(\text{C,O})$ ; blue for  $V(\text{O})$ . Additional figures are shown in the Supporting Information.

between  $V(\text{Ba,C})$  and the core basins C(C) and C(Ba), as previously reported for the Cr(CO)<sub>6</sub> complex, for which the physical origin of metal–CO bonds is different from the common DCD bonding model in TM–CO complexes.<sup>2,23</sup> For values greater than  $\eta = 0.10$ , the different Ba–CO basins separate from each other, as expected because the interaction between CO groups is scarce. At  $\eta = 0.58$ ,  $V(\text{Ba,C})$  separates from the pattern domain, identifying the almost electrostatic character of the Ba–C interaction ( $\eta = 0.5$  is the value which corresponds to an homogeneous electron gas). On the other hand, the C–O covalent bond separates into  $V(\text{O})$  and  $V(\text{C,O})$  only when  $\eta$  reaches the high value of 0.80 (Figure 4). Similar results are obtained for the Ca and Sr complexes 1 and 2. The two-dimensional projection of ELF depicted in Figure 5 for the Ba complex shows that electron pairs are localized close to the valence basins of both metal and carbon atoms (and in the lone pairs of oxygen atoms, as well), where  $\eta \approx 1$ , but scarcely in the regions between Ba and C atoms, where  $\eta$  is close to zero. In fact, the  $\eta$  function has a minimum,

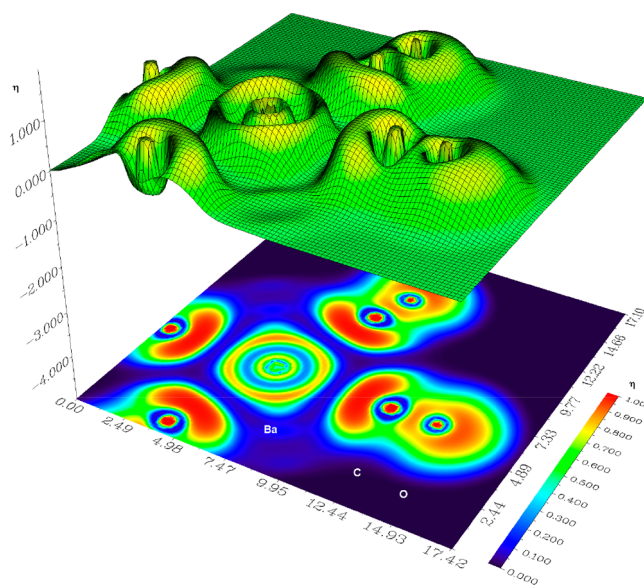


**Figure 5.** Electron localization function projection on a C–Ba–C plane for the Ba(CO)<sub>8</sub> complex (distances in bohrs). Additional figures are shown in the Supporting Information.

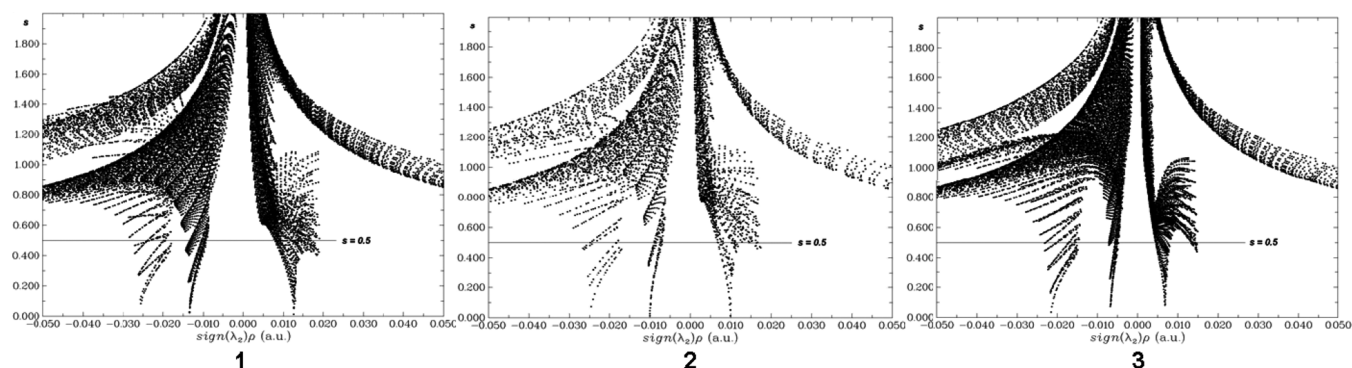


Figure 6. Reduced density gradient ( $s$  function) plotted vs  $\text{sign}(\lambda_2)\rho$  (au) for 1, 2, and 3.

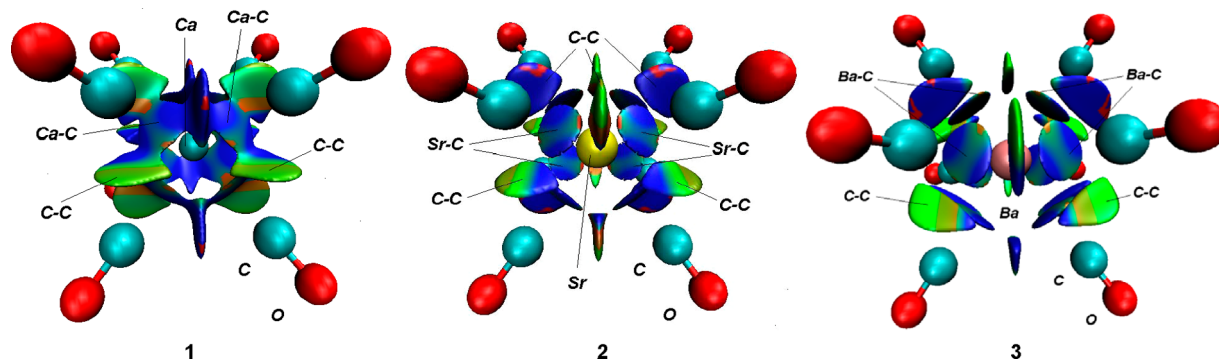


Figure 7. Reduced density gradient isosurfaces ( $s = 0.5$ ) for 1, 2, and 3. Color code: blue (relatively strong attraction;  $\rho > 0$ ,  $\lambda_2 < 0$ ), green (very small attraction or repulsion;  $\rho$  close to 0,  $\lambda_2$  close to 0), red (relatively strong repulsion;  $\rho > 0$ ,  $\lambda_2 > 0$ ).

approximately equal to 0.05 (almost complete delocalization), next to M–C bcps in the three complexes (see Figure S3 in the Supporting Information). In addition, when only  $\pi$  molecular orbitals are taken into account to calculate ELF (a procedure which is commonly known as ELF- $\pi$ ),<sup>22,23</sup> a featureless picture is obtained in the metal–ligand bonding regions of 1–3, showing that only  $\sigma$  MOs contribute to this function in these regions (see Figure S5 in the Supporting Information). This behavior is observed in other functions, too, like in LBO- $\pi$  and WBO- $\pi$ , giving values of 0.001 and 0.058, respectively, for the Ba–C  $\pi$ -bond order (compare with 0.120 and 0.626 in Table 4 for the global bond order), with equivalent results for the other two complexes. When Ba–C bond orders are calculated for the BaCO<sup>+</sup> cation, the following results are obtained: WBO is 1.054 and WBO- $\pi$  is 0.391 (substantial contribution of  $\pi$  MOs), and FBO is 1.030, whereas FBO- $\pi$  is 0.371 (again substantial contribution of  $\pi$  MOs), which are consistent with a relevant  $\pi$ -back-donation in this particular compound.

Two further tools that can be used to characterize interactions like the ones observed in complexes 1–3 are the reduced density gradient method (RDG) and the density overlap region indicator (DORI), which are particularly useful for the analysis of weak interactions as they are two different flavors of the generally called noncovalent interaction index.<sup>24</sup> To distinguish weak interaction regions from other regions in the molecule, the RDG method uses the dimensionless reduced electron density gradient

$$s \equiv \frac{1}{2(3\pi^2)^{1/3}} \frac{|\nabla\rho|}{\rho^{4/3}}$$

which discriminates weak interactions (small  $\rho$ , very small  $\nabla\rho$ , medium  $s$ ) from the rest of interactions in the molecule.

Similarly, the DORI function,  $\gamma \equiv \frac{\theta}{1+\theta}$ , with  $\theta \equiv [\nabla(\nabla\rho/\rho)]^2/(\nabla\rho/\rho)^6$ , is close to 1 in bonding regions and close to 0 at nuclei and far from the molecule, with the particularity that both covalent and noncovalent interactions can be visualized simultaneously (see the Supporting Information, Figure S4). In Figure 6, the RDG of the three complexes is plotted against  $\text{sign}(\lambda_2)\rho$ , where  $\lambda_2$  is the second highest eigenvalue of the electron density's Hessian matrix. The three spikes at the bottom of each plot, which point toward low values of  $\rho$ , reveal the existence of noncovalent interactions in complexes 1–3. By taking the value  $s = 0.5$  (horizontal lines in Figure 6), the isosurfaces depicted in Figure 7 show only the weak interactions and, at the same time, can discriminate between different types of noncovalent interactions, with the strongest ones being those corresponding to M–C bonding interactions ( $\lambda_2$  negative and  $\rho$  between 0.020 and 0.025 au; see Figure 6 and Table 2), whereas the smallest ones ( $\rho$  between 0.005 and 0.010 au; see Figure 6) refer to even weaker intramolecular van der Waals interactions between CO groups, including both attractive (negative  $\lambda_2$ ) and repulsive (positive  $\lambda_2$ ) interactions. As the latter are very small, they do not generate the emergence of bcps or bps between C atoms at the equilibrium geometries. Similarly, a totally symmetric vibration, which preserves the  $O_h$  symmetry (like the one which transforms one theoretically optimized model into the other) does not reveal new bps or bcps. Not surprisingly, a small nonsymmetric perturbation of the geometry (for instance, by opening a single C–M–C angle or stretching a single M–C bond) does lead to the presence of such bps connecting neighboring CO groups, as has been observed previously, for instance, in the Co<sub>2</sub>(CO)<sub>8</sub> complex.<sup>25a</sup> However, it should be emphasized that the presence of bcps and bps *alone* is not a definitive sign of

noncovalent interactions between the C atoms (in the traditional chemical sense), as previous studies have recently shown,<sup>25b</sup> although they may be used to confirm the existence of such interactions revealed by other methods, like the RDG and DORI approaches here utilized.

## CONCLUSIONS

Bonding in alkaline-earth carbonyl complexes  $\text{Ca}(\text{CO})_8$  (1),  $\text{Sr}(\text{CO})_8$  (2), and  $\text{Ba}(\text{CO})_8$  (3) in their ground states ( $T$ ,  $O_h$ ) has been theoretically analyzed using both the quantum theory of atoms in molecules and the electron localization function approaches, through the calculation of several tools related to bond order, bond strength, and covalent/electrostatic character of bonds, among others. The main conclusions obtained from the current study are as follows.

(1) M–CO interactions in 1, 2, and 3 are mainly of electrostatic nature, with an increasing covalent contribution to the energy on going from 1 to 3, which can be estimated in 32% for Ca–CO, 37% for Sr–CO, and 48% for Ba–CO from interacting quantum atom calculations.

(2) The total bond order of M–CO interactions has been estimated to be between 0.50 and 0.60, whereas the covalent contribution to the bond order lies between 0.10 and 0.15, calculated using several partition schemes of the electron density (Laplacian, Wiberg, Mayer's fuzzy, and QTAIM-DI).

(3) No  $\pi$ -back-donation from M to CO has been detected as  $\delta(\text{M}\cdots\text{O}_{\text{CO}})$  delocalization indexes give negligible values; ELF- $\pi$  function gives featureless images in M–CO bonding regions, and  $\pi$  M–C bond orders show values 1 or 2 orders of magnitude lower than those of global bond orders.

(4) Source function calculation, the reduced density gradient method, and the density overlap regions indicator are consistent with closed-shell interactions for the M–CO bonding in the three complexes, with several indexes similar to those found previously in the  $\text{Cr}(\text{CO})_6$  complex (e.g., inadequacy of the simple DCD model), but with some important differences, as well (e.g.,  $H_b/\rho_b > 0$  in 1–3, whereas  $H_b/\rho_b < 0$  in  $\text{Cr}(\text{CO})_6$ ), which traditionally classifies Cr–CO interaction as a dative bond, whereas M–CO bonding in 1–3 shows features typical of strong intramolecular van der Waals interactions or several types of hydrogen bonds.<sup>26</sup>

(5) The noncovalent intramolecular interactions between neighboring CO groups revealed by RDG and DORI approaches are likely to be the origin of the experimentally observed red shifts for the CO stretching frequencies in these complexes. As suggested by the calculated values of  $\delta(\text{C}_{\text{CO}}\cdots\text{C}_{\text{CO}})$  in 1–3, which are not negligible at all, the delocalization of the electron density in each C–O bond toward its three adjacent CO $\cdots$ CO interactions leads to a decrease in the C–O force constant and hence to the experimentally observed red shift of the stretching frequency.

## EXPERIMENTAL SECTION

**Computational Methods.** Theoretically optimized geometries were obtained using two different methods: M06-2X-D3/Def2-TZVPP and B3LYP-D3(BJ)/TZ2P (Table S1). Binding energies, zero-point energy corrections, and CO stretch frequencies for the three complexes using both methods may be seen in the Supporting Information (Tables S6–S8). A fully relativistic four-component Hamiltonian including spin–orbit terms in double-group symmetry, coupled with the hybrid M06-2X and B3LYP-D3(BJ) density functionals,<sup>27</sup> with all-electron relativistic QZ4P basis sets, and including dispersion corrections with Becke–Johnson damping,<sup>28</sup> as implemented in the ADF2012 program package,<sup>29</sup> were used for

single-point electronic structure calculations at the optimized geometries. These first two models are denoted, respectively, SO-M06-2X/QZ4P (model 1) and SO-B3LYP-D3/QZ4P (model 2). In addition, two nonrelativistic models were utilized, as well: M06-D3/6-311++G(3df,3pd),DKH3-QZP (model 3) and B3P86-D3/6-311++G(3df,3pd),DKH3-QZP (model 4), which include, together with a three-parameter empirical dispersion, the all-electron 6-311++G(3df,3pd) basis set for C and O atoms and the relativistic all-electron DKH3-QZP basis set for metal atoms,<sup>30</sup> as implemented in the GAUSSIAN09 program package.<sup>31</sup>

The obtained ground-state electronic wave functions, which were found to be stable, were then used for the QTAIM and ELF calculations, which included both local and integral properties and were carried out with the AIMAll,<sup>32</sup> AIM2000,<sup>33</sup> DGrid,<sup>34</sup> Multiwfn,<sup>35</sup> and Chimera<sup>36</sup> program packages. The accuracy of the local properties was finally set at  $1.0 \times 10^{-10}$  (from the gradient of the electron density at bcps), and that of the integral properties was established at a minimum of  $1.0 \times 10^{-4}$  (from the Laplacian of the integrated electron density).

## ASSOCIATED CONTENT

### Supporting Information

The Supporting Information is available free of charge at <https://pubs.acs.org/doi/10.1021/acs.organomet.9b00699>.

Atomic coordinates of optimized structures in xyz format (Table S1) (XYZ)

Complementary data obtained from the DFT and QTAIM studies (Tables S2–S8), as well as from ELF studies (Figures S1–S5) (PDF)

## AUTHOR INFORMATION

### Corresponding Author

\*E-mail: [fvu@uniovi.es](mailto:fvu@uniovi.es).

### ORCID

Juan F. Van der Maelen: 0000-0002-9528-3423

### Notes

The author declares no competing financial interest.

## ACKNOWLEDGMENTS

This work has been supported by the Spanish MINECO project MAT2016-78155-C2-1-R and the Principality of Asturias Grant No. GRUP-IN-14-060. The author also thanks the reviewers for their valuable contributions.

## REFERENCES

- (1) Crabtree, R. H. *The Organometallic Chemistry of the Transition Metals*; John Wiley & Sons: Hoboken, NJ, 2005.
- (2) Frenking, G.; Fröhlich, N. The Nature of the Bonding in Transition-Metal Compounds. *Chem. Rev.* **2000**, *100*, 717–774.
- (3) Zhou, M.; Andrews, L.; Bauschlicher, C. W., Jr. Spectroscopic and Theoretical Investigations of Vibrational Frequencies in Binary Unsaturated Transition-Metal Carbonyl Cations, Neutrals, and Anions. *Chem. Rev.* **2001**, *101*, 1931–1961.
- (4) Hurlburt, P. K.; Rack, J. J.; Luck, J. S.; Dec, S. F.; Webb, J. D.; Anderson, O. P.; Strauss, S. H. Nonclassical Metal Carbonyls:  $[\text{Ag}(\text{CO})]^+$  and  $[\text{Ag}(\text{CO})_2]^+$ . *J. Am. Chem. Soc.* **1994**, *116*, 10003–10014.
- (5) Mitoraj, M. P.; Michalak, A.; Ziegler, T. A Combined Charge and Energy Decomposition Scheme for Bond Analysis. *J. Chem. Theory Comput.* **2009**, *5*, 962–975.
- (6) Wu, X.; Zhao, L.; Jin, J.; Pan, S.; Li, W.; Jin, X.; Wang, G.; Zhou, M.; Frenking, G. Observation of Alkaline Earth Complexes  $\text{M}(\text{CO})_8$  (M = Ca, Sr, or Ba) that Mimic Transition Metals. *Science* **2018**, *361*, 912–916.

- (7) (a) Landis, C. R.; Hughes, R. P.; Weinhold, F. Comment on "Observation of alkaline earth complexes  $M(\text{CO})_8$  ( $M = \text{Ca}, \text{Sr}, \text{or Ba}$ ) that mimic transition metals. *Science* **2019**, *365*, eaay2355. (b) Zhao, L.; Pan, S.; Zhou, M.; Frenking, G. Response to Comment on "Observation of alkaline earth complexes  $M(\text{CO})_8$  ( $M = \text{Ca}, \text{Sr}, \text{or Ba}$ ) that mimic transition metals. *Science* **2019**, *365*, eaay5021.
- (8) Koch, D.; Chen, Y.; Golub, P.; Manzhos, S. Revisiting  $\pi$  Back-bonding: The Influence of d Orbitals on Metal–CO Bonds and Ligand Red Shifts. *Phys. Chem. Chem. Phys.* **2019**, *21*, 20814–20821.
- (9) (a) Bader, R. F. W. *Atoms in Molecules: A Quantum Theory*; Clarendon Press: Oxford, U.K., 1990. (b) Popelier, P. L. A. *Atoms in Molecules: An Introduction*; Prentice Hall: Upper Saddle River, NJ, 2000. (c) Matta, C. F., Boyd, R. J., Eds. *The Quantum Theory of Atoms in Molecules*; Wiley-VCH: Weinheim, Germany, 2007.
- (10) (a) Gatti, C., Macchi, P., Eds. *Modern Charge Density Analysis*; Springer: Heidelberg, Germany, 2012. (b) Frenking, G., Shaik, S., Eds. *The Chemical Bond*; Wiley-VCH: Weinheim, Germany, 2014.
- (11) Gatti, C.; Lasi, D. Source Function Description of Metal–Metal Bonding in d-block Organometallic Compounds. *Faraday Discuss.* **2007**, *135*, 55–78.
- (12) (a) Popelier, P. L. A.; Kosov, D. S. Atom–Atom Partitioning of Intramolecular and Intermolecular Coulomb Energy. *J. Chem. Phys.* **2001**, *114*, 6539–6547. (b) Blanco, M. A.; Martín Pendás, A.; Francisco, E. Interacting Quantum Atoms: A Correlated Energy Decomposition Scheme Based on the Quantum Theory of Atoms in Molecules. *J. Chem. Theory Comput.* **2005**, *1*, 1096–1109.
- (13) (a) Cortés-Guzmán, F.; Bader, R. F. W. Complementarity of QTAIM and MO Theory in the Study of Bonding in Donor–Acceptor Complexes. *Coord. Chem. Rev.* **2005**, *249*, 633–662. (b) Macchi, P.; Sironi, A. Chemical Bonding in Transition Metal Carbonyl Clusters: Complementary Analysis of Theoretical and Experimental Electron Densities. *Coord. Chem. Rev.* **2003**, *238–239*, 383–412. (c) Lepetit, C.; Fau, P.; Fajferweg, K.; Kahn, M. L.; Silvi, B. Topological Analysis of the Metal–Metal Bond: A Tutorial Review. *Coord. Chem. Rev.* **2017**, *345*, 150–181. (d) Gatti, C. Chemical Bonding in Crystals: New Directions. *Z. Kristallogr. - Cryst. Mater.* **2005**, *220*, 399–457. (e) Shahbazian, S. Why Bond Critical Points Are Not "Bond" Critical Points. *Chem. - Eur. J.* **2018**, *24*, 5401–5405.
- (14) Reiher, M.; Wolf, A. *Relativistic Quantum Chemistry: The Fundamental Theory of Molecular Science*; Wiley-VCH: Weinheim, Germany, 2009.
- (15) (a) Cabeza, J. A.; Van der Maelen, J. F.; García-Granda, S. Topological Analysis of the Electron Density in the N-Heterocyclic Carbene Triruthenium Cluster  $[\text{Ru}_3(\mu\text{-H})_2(\mu^3\text{-MeImCH})(\text{CO})_9]$  ( $\text{Me}_2\text{Im} = 1,3\text{-Dimethylimidazol-2-ylidene}$ ). *Organometallics* **2009**, *28*, 3666–3672. (b) Van der Maelen, J. F.; Cabeza, J. A. A QTAIM Analysis of the Bonding in Mo–Mo Bonded Dimolybdenum Complexes. *Inorg. Chem.* **2012**, *51*, 7384–7391. (c) Cabeza, J. A.; Fernández-Colinas, J. M.; García-Álvarez, P.; Pérez-Carreño, E.; Pruneda, V.; Van der Maelen, J. F. Deprotonation of C-Alkyl Groups of Cationic Triruthenium Clusters Containing Cyclometalated C-Alkylpyrazinium Ligands: Experimental and Computational Studies. *Chem. - Eur. J.* **2013**, *19*, 9251–9260. (d) Brugos, J.; Cabeza, J. A.; García-Álvarez, P.; Kennedy, A. R.; Pérez-Carreño, E.; Van der Maelen, J. F. 2-(Methylamido)pyridine–Borane: A Tripod  $\kappa^3\text{N,H,H}$  Ligand in Trigonal Bipyramidal Rhodium(I) and Iridium(I) Complexes with an Asymmetric Coordination of its  $\text{BH}_3$  Group. *Inorg. Chem.* **2016**, *55*, 8905–8912. (e) Brugos, J.; Cabeza, J. A.; García-Álvarez, P.; Pérez-Carreño, E.; Van der Maelen, J. F. Octahedral Manganese(I) and Ruthenium(II) Complexes Containing 2-(Methylamido)pyridine–Borane as a Tripod  $\kappa^3\text{N,H,H}$ -Ligand. *Dalton Trans* **2017**, *46*, 4009–4017. (f) Van der Maelen, J. F.; Cabeza, J. A. A Topological Analysis of the Bonding in  $[\text{M}_2(\text{CO})_{10}]$  and  $[\text{M}_3(\mu\text{-H})_3(\text{CO})_{12}]$  complexes ( $M = \text{Mn}, \text{Tc}, \text{Re}$ ). *Theor. Chem. Acc.* **2016**, *135*, 64. (g) Van der Maelen, J. F.; García-Granda, S.; Cabeza, J. A. Theoretical Topological Analysis of the Electron Density in a Series of Triosmium Carbonyl Clusters:  $[\text{Os}_3(\text{CO})_{12}]$ ,  $[\text{Os}_3(\mu\text{-H})_2(\text{CO})_{10}]$ ,  $[\text{Os}_3(\mu\text{-H})(\mu\text{-OH})(\text{CO})_{10}]$ , and  $[\text{Os}_3(\mu\text{-H})(\mu\text{-Cl})(\text{CO})_{10}]$ . *Comput. Theor. Chem.* **2011**, *968*, 55–63. (h) Ruiz, J.; Sol, D.; García, L.; Mateo, M. A.; Vivanco, M.; Van der Maelen, J. F. Generation and Tunable Cyclization of Formamidinate Ligands in Carbonyl Complexes of Mn(I): An Experimental and Theoretical Study. *Organometallics* **2019**, *38*, 916–925. (i) Van der Maelen, J. F.; Brugos, J.; García-Álvarez, P.; Cabeza, J. A. Two Octahedral  $\sigma$ -borane Metal (MnI and RuII) Complexes Containing a Tripod  $\kappa^3\text{N,H,H}$ -ligand: Synthesis, Structural Characterization, and Theoretical Topological Study of the Charge Density. *J. Mol. Struct.* **2020**, *1201*, 127217. (j) Tiana, D.; Francisco, E.; Blanco, M. A.; Macchi, P.; Sironi, A.; Martín-Pendás, A. Bonding in Classical and Nonclassical Transition Metal Carbonyls: The Interacting Quantum Atoms Perspective. *J. Chem. Theory Comput.* **2010**, *6*, 1064–1074. (k) Wu, X.; Zhao, L.; Jiang, D.; Fernández, I.; Berger, R.; Zhou, M.; Frenking, G. Barium as Honorary Transition Metal in Action: Experimental and Theoretical Study of  $\text{Ba}(\text{CO})^+$  and  $\text{Ba}(\text{CO})^-$ . *Angew. Chem., Int. Ed.* **2018**, *57*, 3974–3980. (l) Mayer, I.; Salvador, P. Overlap Populations, Bond Orders and Valences for 'Fuzzy' Atoms. *Chem. Phys. Lett.* **2004**, *383*, 368–375. (m) Mayer, I. *Bond Orders and Energy Components: Extracting Chemical Information from Molecular Wave Functions*; CRC Press: Boca Raton, FL, 2016. (n) Lu, T.; Chen, F. Bond Order Analysis Based on the Laplacian of Electron Density in Fuzzy Overlap Space. *J. Phys. Chem. A* **2013**, *117*, 3100–3108. (o) Wiberg, K. B. Application of the Pople–Santry–Segal CNDO Method to the Cyclopropylcarbonyl and Cyclobutyl Cation and to Bicyclobutane. *Tetrahedron* **1968**, *24*, 1083–1096. (p) Tiana, D.; Francisco, E.; Blanco, M. A.; Macchi, P.; Sironi, A.; Martín-Pendás, A. Restoring Orbital Thinking from Real Space Descriptions: Bonding in Classical and Non-classical Transition Metal Carbonyls. *Phys. Chem. Chem. Phys.* **2011**, *13*, 5068–5077. (q) Racioppi, S.; Della Pergola, R.; Colombo, V.; Sironi, A.; Macchi, P. Electron Density Analysis of Metal Clusters with Semi-Interstitial Main Group Atoms. Chemical Bonding in  $[\text{Co}_6\text{X}(\text{CO})_{16}]^-$  Species. *J. Phys. Chem. A* **2018**, *122*, 5004–5015. (r) Becke, A. D.; Edgecombe, K. E. A Simple Measure of Electron Localization in Atomic and Molecular Systems. *J. Chem. Phys.* **1990**, *92*, 5397–5403. (s) (a) Davidson, E. R.; Kunze, K. L.; Machado, F. B. C.; Chakravorty, S. J. The Transition Metal–Carbonyl Bond. *Acc. Chem. Res.* **1993**, *26*, 628–635. (b) Matito, E.; Solà, M. The Role of Electronic Delocalization in Transition Metal Complexes from the Electron Localization Function and the Quantum Theory of Atoms in Molecules Viewpoints. *Coord. Chem. Rev.* **2009**, *253*, 647–665. (t) (a) Johnson, E. R.; Keinan, S.; Mori-Sánchez, P.; Contreras-García, J.; Cohen, A. J.; Yang, W. Revealing Noncovalent Interactions. *J. Am. Chem. Soc.* **2010**, *132*, 6498–6506. (b) de Silva, P.; Corminboeuf, C. Simultaneous Visualization of Covalent and Noncovalent Interactions Using Regions of Density Overlap. *J. Chem. Theory Comput.* **2014**, *10*, 3745–3756. (c) Pastorczak, E.; Corminboeuf, C. Perspective: Found in translation: Quantum Chemical Tools for Grasping Non-covalent Interactions. *J. Chem. Phys.* **2017**, *146*, 120901. (u) (a) Foroutan-Nejad, C.; Shahbazian, S.; Marek, R. Toward a Consistent Interpretation of the QTAIM: Tortuous Link Between Chemical Bonds, Interactions, and Bond/Line Paths. *Chem. - Eur. J.* **2014**, *20*, 10140–10152. (b) Jabłoński, M. On the Uselessness of Bond Paths Linking Distant Atoms and on the Violation of the Concept of Privileged Exchange Channels. *ChemistryOpen* **2019**, *8*, 497–507. (v) Grabowski, S. J. What Is the Covalency of Hydrogen Bonding? *Chem. Rev.* **2011**, *111*, 2597–2625. (w) (a) Zhao, Y.; Truhlar, D. G. The M06 Suite of Density Functionals for Main Group Thermochemistry, Thermochemical Kinetics, Noncovalent Interactions, Excited States, and Transition Elements: Two New Functionals and Systematic Testing of Four M06-class Functionals and 12 Other Functionals. *Theor. Chem. Acc.* **2008**, *120*, 215–241. (b) Lee, C.; Yang, W.; Parr, R. G. Development of the Colle-Salvetti Correlation-Energy Formula into a Functional of

the Electron Density. *Phys. Rev. B: Condens. Matter Mater. Phys.* **1988**, *37*, 785–789. (c) Perdew, J. P. Density-Functional Approximation for the Correlation Energy of the Inhomogeneous Electron Gas. *Phys. Rev. B: Condens. Matter Mater. Phys.* **1986**, *33*, 8822–8824.

(28) Grimme, S.; Ehrlich, S.; Goerigk, L. Effect of the Damping Function in Dispersion Corrected Density Functional Theory. *J. Comput. Chem.* **2011**, *32*, 1456–1465.

(29) Baerends, E. J.; Ziegler, T.; Autschbach, J.; Bashford, D.; Bérces, A.; Bickelhaupt, F. M.; Bo, C.; Boerrigter, P. M.; Cavallo, L.; Chong, D. P.; Deng, L.; Dickson, R. M.; Ellis, D. E.; van Faassen, M.; Fan, L.; Fischer, T. H.; Fonseca-Guerra, C.; Ghysels, A.; Giammona, A.; van Gisbergen, S. J. A.; Götz, A. W.; Groeneveld, J. A.; Gritsenko, O. V.; Grüning, M.; Gusarov, S.; Harris, F. E.; van den Hoek, P.; Jacob, C. R.; Jacobsen, H.; Jensen, L.; Kaminski, J. W.; van Kessel, G.; Kootstra, F.; Kovalenko, A.; Krykunov, M. V.; van Lenthe, E.; McCormack, D. A.; Michalak, A.; Mitoraj, M.; Neugebauer, J.; Nicu, V. P.; Noodleman, L.; Osinga, V. P.; Patchkovskii, S.; Philipsen, P. H. T.; Post, D.; Pye, C. C.; Ravenek, W.; Rodriguez, J. I.; Ros, P.; Schipper, P. R. T.; Schreckenbach, G.; Seldenthuis, J. S.; Seth, M.; Snijders, J. G.; Solà, M.; Swart, M.; Swerhone, D.; te Velde, G.; Vernooijs, P.; Versluis, L.; Visscher, L.; Visser, O.; Wang, F.; Wesolowski, T. A.; van Wezenbeek, E. M.; Wiesenekker, G.; Wolff, S. K.; Woo, T. K.; Yakovlev, A. L. *ADF2012*, revision 01d; SCM; Theoretical Chemistry; Vrije Universiteit: Amsterdam, The Netherlands, 2012.

(30) (a) Noro, T.; Sekiya, M.; Koga, T. Sapporo-(DKH3)-nZP (n = D, T, Q) Sets for the Sixth Period s-, d-, and p-block Atoms. *Theor. Chem. Acc.* **2013**, *132*, 1363. (b) Noro, T.; Sekiya, M.; Koga, T. Segmented Contracted Basis Sets for Atoms H Through Xe: Sapporo-(DK)-nZP sets (n = D, T, Q). *Theor. Chem. Acc.* **2012**, *131*, 1124.

(31) Frisch, M. J.; Trucks, G. W.; Schlegel, H. B.; Scuseria, G. E.; Robb, M. A.; Cheeseman, J. R.; Scalmani, G.; Barone, V.; Mennucci, B.; Petersson, G. A.; Nakatsuji, H.; Caricato, M.; Li, X.; Hratchian, H. P.; Izmaylov, A. F.; Bloino, J.; Zheng, G.; Sonnenberg, J. L.; Hada, M.; Ehara, M.; Toyota, K.; Fukuda, R.; Hasegawa, J.; Ishida, M.; Nakajima, T.; Honda, Y.; Kitao, O.; Nakai, H.; Vreven, T.; Montgomery, J. A., Jr.; Peralta, J. E.; Ogliaro, F.; Bearpark, M.; Heyd, J. J.; Brothers, E.; Kudin, K. N.; Staroverov, V. N.; Kobayashi, R.; Normand, J.; Raghavachari, K.; Rendell, A.; Burant, J. C.; Iyengar, S. S.; Tomasi, J.; Cossi, M.; Rega, N.; Millam, J. M.; Klene, M.; Knox, J. E.; Cross, J. B.; Bakken, V.; Adamo, C.; Jaramillo, J.; Gomperts, R.; Stratmann, R. E.; Yazyev, O.; Austin, A. J.; Cammi, R.; Pomelli, C.; Ochterski, J. W.; Martin, R. L.; Morokuma, K.; Zakrzewski, V. G.; Voth, G. A.; Salvador, P.; Dannenberg, J. J.; Dapprich, S.; Daniels, A. D.; Farkas, O.; Foresman, J. B.; Ortiz, J. V.; Cioslowski, J.; Fox, D. J. *Gaussian 09*, revision B.01; Gaussian, Inc.: Wallingford, CT, 2009.

(32) Keith, T. A. *AIMAll*, version 15.09.27; TK Gristmill Software: Overland Park, KS, 2015.

(33) Biegler-König, F.; Schönbohm, J. Update of the AIM2000-program for Atoms in Molecules. *J. Comput. Chem.* **2002**, *23*, 1489–1494.

(34) Kohout, M. *DGrid-4.6*; Max Planck Institute for Physical Chemistry of Solids: Dresden, Germany, 2011.

(35) Lu, T.; Chen, F. Multiwfn: A Multifunctional Wavefunction Analyzer. *J. Comput. Chem.* **2012**, *33*, 580–592.

(36) Pettersen, E. F.; Goddard, T. D.; Huang, C. C.; Couch, G. S.; Greenblatt, D. M.; Meng, E. C.; Ferrin, T. E. UCSF Chimera-A Visualization System for Exploratory Research and Analysis. *J. Comput. Chem.* **2004**, *25*, 1605–1612.